Kaupp, J Material Sci Eng 2018, 7:4
DOI: 10.4172/2169-0022.1000473

Journal of Material Sciences & Engineering

Research Article Open Access

Six Polymorphs of Sodium Chloride upon Depth-Sensing Macroindentation with Unusual Long-Range Cracks Requiring 30 N Load

Gerd Kaupp*

University of Oldenburg, Edewecht, Oldenburg, Germany

Abstract

A sodium chloride single crystal is depth-sensing indented with a Vickers indenter at a Zwick/Roell ZHV Zwicky Z2.5 macro region instrument, together with Stephanie Rösner from Zwick GmbH & Co KG, Ulm, Germany. Normal forces up to 50 N load and 120 µm depth are applied, to experimentally secure the onsets of known and to locate new phase-changes with direct linear regression analyses, avoiding iterations. The author's physically deduced universal eqns. (1-7) are used for the data analyses. Four sharp phase-change onsets could thus be experimentally located, revealing four new polymorphs of NaCl in addition to the long known fcc and bcc polymorphs. Their relation to the three theoretically predicted higher pressure crystal structures in Reference is thus not clear. The predicted metallic character is unclear: no color formation or metallic reflection was observed by the author up to 50 N loads. No cracking of any type occurs at the indenter tip, but a new type of long-range cracking at the 30 N ranges occurred, and its highly resolved microscopy reveal two-step nucleation from a polymorphs' interface exit. Inverted 3D microscopy of the residual impressions of the author with his Keyence VHX 100 microscope reveals crystallization of halite cubes upon unloading. The physical hardness increases (factor 5.9), the physical indentation modulus decreases (factor 2.3) upon load. The indentation phase-transformation energies cover 7 powers of 10. These data question the reliability of non-depth-sensing ISO/ASTM Standards of industrial Vickers, Brinell, and Rockwell, etc hardness parameters, as they cannot consider inevitable multiple phase-changes at very high loads, do not characterize the pristine rather than phase-transformed industrial material (including super-alloys), and miss the permissible pressure stress for avoiding phase changes. The risk of failure by nucleation of cracks at polymorph interfaces requires depth-sensing. Deviations from the mathematically required 5/4 ratio of applied-work over indentation-work are a rapid means to reveal phase-changes from old published loading curves by their graphical integration.

Keywords: 3D-Microscope; 3D Impression shape; 5 Consecutive phase-changes; Consequences for Vickers Hardness; Far distance crack nucleation; Far-distance effects; Favorable model; High pressure depth-sensing indentation; Indentation work; Kaupp-plot; Linear regression; Metallization problem; New cracking behavior; Physical hardness; Physical modulus; Sodium chloride

Introduction

The mechanical properties of sodium chloride belong to the most studied ones. Also the possibility for its phase-transition above the well-known B1 (Halite, fcc, Fm3m) to B2 (bcc, Pm3m) into more energetic ionic polymorphs with predicted metallic character ("above 584 GPa via indirect band-gap closure") have been calculated: Cmcm, Imm, and Pbcm structures at increasing pressure ranges and formation enthalpies [1]. However, experimental proof is still missing. Only one higher energy phase-transition (to give #3 in the following discussion) had been extracted from a published experimental Vickers indentation diagram of NaCl [2]. The linearization is the physically deduced "Kaupp-plot" (so scolded by skeptic iteration experts) (F_N=k $h^{3/2}$), as calculated from the experimental F_N versus h loading plot [3]. It had revealed a kink discontinuity at 2.5 N, which was attributed to the #3 polymorph (perhaps CrB type?) under pressure [4], provided repeatability of the work [2]. Thus, the repetition experiment was necessary, because the paper of [2] contains several inconsistencies: multi-parameter iterations using ISO-14577 h_c from $E_{r\text{-}ISO}$=50 GPa iteration, followed by a second-order polynomial with α_{eff}=70.4°, and "R_{eff}=3.3 µm" for a "sharp" Vickers indenter were used for the construction of an unphysical "F_N versus h^2 relation", or pileup was mentioned but it is not discernable in the provided images or the figure refers to *in situ* values for NaCl up to post-indentation values up to 45 N (!) with error bars as "calculated from *P-h* data" [2]. Apparently, this tried to substantiate an (unphysical) "F_N versus h^2 relation", whereas the maximal load was only 4.6 N. That is more than puzzling! Phase-changes were not considered [2]. All of that requires an experimental check for reproduction, in order to secure the result of our physical analysis that found a sharp kink at 2.5 N by a phase-change. Furthermore, it was to be checked whether further increased load would allow the detection of further polymorphs with metallization of sodium chloride by local color change with a metallic reflection [4,5]. Also, the reproduction with the elucidation of any cracking appeared necessary. The thermal conductivity of the fcc NaCl at 298 K is 4.6 W/m K [6]. This is relatively high for a non-metal so that we do not expect significant temperature increase during the endothermic phase-transitions upon the indentation. Also the thermal expansion (44 10^{-6}/K) of the fcc [6] and bcc phase at 30 GPa are rather low [7]. The activation energy of the fcc to bcc transition (from RT to 400°C) is 0.001716 µJ/µN [4]. The physical hardness H_{phys} is the normalized energy-corrected indentation resistance k for conical/pyramidal indenters [2]. That is general for Vickers indenter with H_{phys}=0.0325745 k, where k is the penetration resistance (the slope of the so-called Kaupp-plot) from F_N=k $h^{3/2}$ (Figure 1).

Materials and Methods

A drilled 40.3 23.0 6.3 mm^3 two sides polished sodium chloride mono-crystal window plate from Alpha Aesar Thermo Fischer GmbH,

***Corresponding author:** Gerd Kaupp, University of Oldenburg, Diekweg 15, D-26188 Edewecht, Oldenburg, Germany, Tel: +49 (0)441/7983842; E-mail: gerd.kaupp@uni-oldenburg.de

Received July 23, 2018; **Accepted** August 01, 2018; **Published** August 10, 2018

Citation: Kaupp G (2018) Six Polymorphs of Sodium Chloride upon Depth-Sensing Macroindentation with Unusual Long-Range Cracks Requiring 30 N Load. J Material Sci Eng 7: 473. doi: 10.4172/2169-0022.1000473

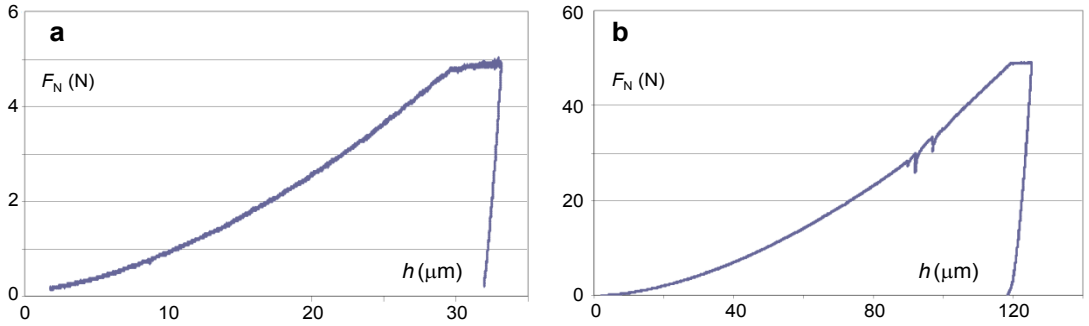

Figure 1: Indentation force-depth curves on NaCl (a) up to 5 N and (b) up to 50 N with a minor depression at 28.5 N and main depressions at 29.8 and 34.0 N loads that are also seen in the linearized F_N versus $h^{3/2}$ plot (Figure 2). They indicate the formation of very distant cracks.

Kandel, Germany was used for the indentations at (for technical reasons) 2.5-3.5 mm distance from the sides. 3 at least 5 mm distant in-dentations at 5 N loads were averaged. One indentation each was performed displaced at opposing sides for 20 and 50 N loads. The kinks have been calculated from the linear branches' trend lines with >0.999 correlation coefficients. The displacement controlled measurements used a depth sensing Zwick/Roell ZHV Zwicky Z2.5 macro region instrument according to ISO 14577 with compliance of 0.0046985 μm/N at 1 μm/s load and unload rates, and unloads after 30 s hold periods, in the open air by the sample in the ambient atmosphere. The calibrated Vickers indenter (E 27781, MPA Stuttgart, Germany (DIN EN ISO 6507-2) withstood "the functional requirements within the allowed limits". A 3D digital optical microscope Keyence VHX 100 with a lens providing the 500X to 5000X enlargement range was used with a CCD-camera at almost uniform coaxial vertical (surjective) illumination through an optical fiber in the open air. The separate 25X lens was not adapted to the 3D-facility. The light of a halogen lamp was coaxially reflected back by the sample in ambient atmosphere through a half mirror along the illumination axis into an optical fiber, sending the signals for digital imaging. Equidistant focal images at either 1 or 5 μm distance were taken under automatic position correction. The Keyence software composed these to 3D-images or projections therefrom. As the indentations and microscopy were performed in ambient atmosphere, control images were performed after 10 months storage in a closed box in the air with the silica drying grain of Alpha Aesar, to check the stability of the features.

The data analysis for indentations with pyramidal or conical indenters used the physically founded "Kaupp-plot" (normal force versus depth$^{3/2}$; $F_N=k\ h^{3/2}$ relation) (1) (Figure 2), the energy law-corrected universal indentation hardness H_{phys} [8], and also the energy corrected indentation modulus $E_{r\text{-}phys}$, all without any free-parameter iterations or polynomials or curve fittings [3,8,9]. Everything started with the penetration resistance values k (the slope of the so called Kaupp-plot) before and after the sharp kink onsets at the intersections of the calculated regression lines. Sectional integrations with respect to phase-changes obtained indentation work W_{indent}, applied work $W_{applied}$, and by energy balance the phase-transition energy $W_{transition}$. Only these known physically deduced eqns. (1-7) were used for the calculations [3,4,8,10-12]. The effective semi-angle of the Vickers indenter tip is α=70.32°. F_a is the correction for any axis-cut. The linear regression lines are calculated with Excel(R) in their regions. The correlation coefficient was always r>0.999. The linear red regression lines in Figure 2 are hand-drawn along the plot branches for visualization. The unloading stiffness S, as obtained from the slope at maximal force of the loading force F_{max}, is obtained from the regression of the first linear points (with 100 to 500, mostly 200 points) of the original unloading data. The factor 0.8 is necessary for complying with the energy law, because the depth and volume have been created only with 0.8 F_N [5,9]. The use of eqn. (3) for $E_{r\text{-}phys}$ is continued, because the similar formula for $E_{r\text{-}phys}$ in [8,10] is over-corrected with respect to incorrect $E_{r\text{-}ISO}$, when directly using the experimental stiffness S at peak load of the unloading curve. Eqns. (5-7) are the physical deductions for the applied energy, for obtaining the energetic balance as phase-transition energy [5]. Due to the exponents and differences, the calculations used up to 9 numerals after the decimal point with a pocket calculator, followed by reasonable rounding at the end results.

$$F_N=k\ h^{3/2}+F_a \quad (1)$$

$$H_{phys}=0.8\ k/\pi\ \mathrm{tg}\ \alpha^2\ [\mathrm{mN/\mu m^{3/2}}] \quad (2)$$

$$E_{r\text{-}phys}=0.8\ S/2h_{max}\ \mathrm{tg}\ \alpha\ [\mathrm{mN/\mu m^2}] \quad (3)$$

$$W_{indent}=0.4\ k\ (h^{5/2}-h_{kink}{}^{5/2})+Fa\ (h-h_{kink}) \quad (4)$$

$$W_{applied}=1.25\ W_{indent} \quad (5)$$

$$W_{transition}=\mathrm{full}\ W_{applied}-\Sigma\ (W_{applied})_n \quad (6)$$

$$\mathrm{full}\ W_{applied}=0.5\ F_{N\text{-}max}\ h_{max} \quad (7).$$

All eqns. (2-7) derive from the principal eqn. (1), where h is the penetration depth. The linear Kaupp-plot according to eqn. (1) reveals all initial surface effects by axis cut F_a for correction, and all exothermic or endothermic phase transition onsets as kinks between linear branches if these occur at the chosen load-ranges (Figure 2).

The eqns. (1-7) are not reproducing the long history of conical indentations. The first trial was the Boussinesq's problem of 1885 that found two different mathematical solutions in 1939 and 1965, but both with an exponent 2 on h instead of 3/2 as in eqn. (1). The result from reference [15] was taken up from Oliver-Pharr and this became the basis for ISO 14577 with annual refinements and extensions, but still keeping with the exponent 2, 4 which is however at variance with experimental loading parabolas [15-17]. All of these did not appreciate that the normal force is not only used for creating a volume but also for creating pressure to the environment of such volume. Due to the thus wrong exponent 2 on h, polynomial iterations are required for fitting the load/depth parabolas, be there phase changes or none of them at the chosen loading ranges. Only most finite element simulations are made to converge with h^2, but these fail [12]. Unfortunately, the software of instrument builders must apparently obey to the false ISO standards with the Oliver-Pharr multi-parameter iterations for the measurement of H_{ISO} and $E_{r\text{-}ISO}$. As long as eqn. (1) was only empirically secured by the exponent analysis of loading curves there was a strange objection against

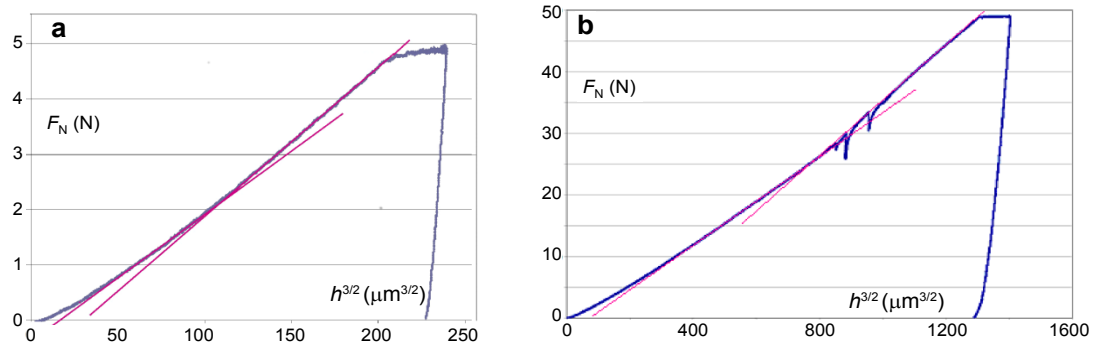

Figure 2: Linearized loading curves (Kaupp-plots) (F_N versus $h^{3/2}$) at (a) 5 and (b) 50 N load, showing in red the linear branches that intersect at the phase-transition points (a) average at 2.487 N, (b) at 24.428 N.

eqn. (1) with the absurd construction of the transformation kink from a line between two points of a poor very blunt indenter measurement with the second linear branch, instead of between the also there depicted extended first and second linear branches [19]. They advocated the fitting of the whole loading curve instead, without separating out their considerable initial effect, by using broken exponents (e.g., exponent 1.75285 or 1.82723) for different parts of the loading parabola and thus acknowledging the very odd dimensions of such parabola constants. This failure encouraged another defaming publication in 2014 with an equally undue trial to degrade the physically correct "Kaupp plot" as "Kaupp-fitting" [20]. But the "Kaupp-plot" using eqn. (1) excludes all data-treatment, and it is therefore totally different from these author's iterative polynomial data fitting procedures. They tried with a strange so-called "Theoretical Confirmation of the exponent 2 on *h*", which is far away from any scientific deduction, by including the result in their "deduction" of their "theoretical confirmation", and they did not consider the excellent opposing curves [12]. It is unscientific to use a definition of hardness H_{ISO} that includes the (false) exponent 2 on h (the hardness is the constant in the force-depth relation!) in connection with an also defined projected contact area $A_c \propto h^2$, for reaching H=P/A_c giving $P \propto h^2$ as already defined in the definitions. The capital error in these definitions is their energy law violation, by not considering the energy for the pressure generation (a parabola with the false exponent 2 would require 33% of the applied indentation energy that cannot be obtained from nothing [5,8]. With other words: the coupling of volume formation with pressure formation is again totally disregarded [20]. Both factors require work that comes from the normal force *P* we call it F_N [5,8].

These invalid allegations have been finally overcome by the physical deductions of the energetic situation in 2013 and of the exponent 3/2 as published in 2016 [3,5]. The scientifically valid deduction of the exponent on *h* of the force-depth loading curve starts with normal force $F_N=k\ h^x$. Reference [3] rightfully combines the components of the normally applied force F_N with $F_N=F_{Np}{}^m F_{Nv}{}^n$ (p for pressure, v for volume). The total pressure (*p*+loss of *p* by plasticization, etc) is $p_{total} \propto V_{cone}$ [3]. With the volume $V_{cone}=\pi\ (\tan\alpha)^2\ h^3/3$ it follows p_{total} and thus also $F_{Np}{}^m \propto h^3$ that is lost for the penetration. With $h=F_{Np}{}^{1/3}$ one obtains the exponent m=1/3 for $F_{Np}{}^m$, and thus also the exponent n=2/3 for $F_{Nv}{}^n$. Therefore (after conversion), $F_{Nv}=k\ h^{3/2}$, which had to be deduced. It is a universal physical law with mathematical precision [3]. The physical indentation hardness H_{phys} of eqn. (2) scales the penetration resistance *k* (the slope of the so-called Kaupp-plot) to the effective half-angle of the pyramid or cone, so that H_{phys} becomes independent of the indenter geometry [8,9]. The here printed eqn. (4) contains also the obvious extensions for the case of phase change. The linearly applied work is $W_{applied}=0.5\ F_{Nmax}\ h_{max}$ from where it follows with the indentation work $W_{indent}=0.4\ k\ h^{5/2}$ and eqn. (1) that $W_{applied}=1.25\ W_{indent}$ in eqn. (5). Thus, eqn. (1) mathematically quantifies 20% of the lost work (a property of every parabola with exponent 3/2) and thus also the lost normal force of F_N for the indentation [5,8]. This explains the factor 0.8 in the eqns. (2) and (3). Transition energies from phase changes (new phases have different *k* values) are the energy balance as in eqn. (6). Eqn. (7) is a special case of eqns. (3) and (5) is deduced [5,9].

Results

Hardness, modulus, and polymorphs

The ISO standard 14577 for pyramidal indentations violates the first energy law and denies physical dimensions. The analysis of loading curves (F_N versus *h*) (Figure 1) according to the Kaupp-plot ($F_N=k\ h^{3/2}$) (Figure 2) recognizes phase-change onsets by sharp kink unsteadiness only in the linearized loading curves with the correct exponent 3/2 [3,8]. The physical hardness is obtained without complications from the penetration resistance *k* (the slope of the so called Kaupp-plot) eqn. (2) and the reduced modulus directly from stiffness *S* and h_{max} according to eqn. (3) (without one with 3 and one with up to 8 free-parameter iterations of ISO) [9]. Different polymorphs must have different hardness and elasticity [9]. The H_{phys} values in Table 1 vary by a factor of 5.939, the indentation moduli by a factor 2.246. However, the meaning of the latter must be considered with care, as multiply phase transitioned polymorphs are unloaded, the reversion rates of which are unknown. There is no modulus value for the halite (fcc) and for #5 in Table 1, as unloading curves within their load ranges for the present conditions are lacking. But such values cannot be easily judged due to the expected strong enhancement of elastic moduli at increasing pressure (the tabulated Young's modulus of 50 GPa for fcc NaCl cannot be compared) [21]. The physically deduced $E_{r\text{-}phys}$ (3) definition stays as close as possible to the unphysical $E_{r\text{-}ISO}$ definition. However both are not Young's moduli. They are "indentation moduli". Young's moduli are strictly unidirectional [9]. This restricts the general value of indentation moduli, even though they belong to the most cited and used values from indentations. Nevertheless, the $E_{r\text{-}phys}$ sizes are listed.

Table 1 shows the *k*-values (penetration resistances) and transition onsets with the H_{phys}-values. The values of *k* and thus H_{phys} increase by a factor of 5.939 and indicate four phase-changes though at very different normal force ranges from 10 mN to 50 N. Their discussion must take into account that the polymorphs exist between their kinks pressures, which are often disregarded.

The NaCl transition onsets	*k*-values (mN/μm$^{3/2}$) and F_a (N)	$F_{N\ kink}$ (N)	H_{phys}=0.8 *k*/ (π tg α^2) (mN/μm$^{3/2}$)	$E_{r\text{-}phys}$=0.8 *S*/(2 h_{max} tg α) (mN/μm^2)	W_{indent}=0.4 *k* ($h_2^{5/2}$−$h_1^{5/2}$)+F_a ·(h_2−h_1) (Nμm)	Normalized W_{indent} (Nμm/N)
fcc to kink[a]	4.1014; 0. 000067	0.000618	0.2408	n.a.[b]	0.000038908	0.06296
fcc to bcc[a]	6.6796; 0.0005632	0.003397	0.2724	32.245	0.00076675	0.2759
bcc to #3[c]	28.2; 0.0222	2.4870[d]	0.7427	21.617	21.9236	8.6668
#3 to #4	33.8; −0.6964	9.1186	1.101	17.698	136.1690	20.533
#4 to #5	35.6; −1.0890	24.4284	1.160	n.a.[b]	604.6890	39.5121
#5 up to 50N (part of #6)	43.9; −8.3251	up to 50	1.430	14.356	1404.5208	54.925

[a]Indented with Berkovich [4];

[b]Not available; a first principle calculation predicts bulk moduli of 27.117 GPa for fcc-NaCl and 27.934 GPa for bcc NaCl at zero pressure [21];

[c]This polymorph was assumed to be the bcc NaCl [3] but already corrected [4];

[d]This reproduces the 2.5 N value at 21.1μm depth [3] as had been extracted from the published loading curve of [2].

Table 1: Mechanical data of depth sensing Vickers indentations onto an optical NaCl window plate, including the physical indentation work.

The pristine materials' values have to be taken at loads before the first phase-change kink that has to be detected with eqn. (1) and Kaupp-plot. For example, the Figures 1a and 1b with F_N versus h do not recognize phase-transition onsets. These are only revealed by the Kaupp-plots in Figure 2 according to eqn. (1), as exemplified for the 5 and 50 N impressions, The kinks are clearly seen there, but the ranges of fcc to bcc are almost hidden at the 5 N ranges and require the corresponding plots at much lower force that are not displayed here (Table 1).

The validity of the NaCl loading curve [2] could be confirmed. Its residual impression diameter (ca 225 μm at 4.3 N) compares favorably with the present one (243.73 μm after 5.0 N load). Also the second transition onsets at 21.096 μm and 2.5 N, as calculated from the loading curve data [2] and published [4,5] comply excellent with the 20.8076 μm and 2.487 ± 0,05 N values in Tables 1 and 2. This confirms the first experimental proof of a third NaCl polymorph at high pressure since 2013. The fcc to bcc transition of NaCl of [4] is also present in Figure 2a, but not precisely accessible at the scale of 5 N. Figures 1b and 2b demonstrate the situation with the 50 N indents. The depressions in the 30 N regions locate the cracking onsets. These cracks are not radial or horizontal at the indenter but far-away long-range and they do not disturb the linear branch as depicted with the upper thin red line (the depression points are of course not part of the regression). Interestingly, the second through fifth phase-changes from the 5, 20, and 50 N impressions did not exhibit a color change or metallic reflection down to 120 mm (Tables 1 and 2), as should be expected for metals, but electric conductance measurements during indentation of NaCl are additionally planned.

Phase-transition work

Table 1 also contains the indentation works (4) for their stability ranges (for #6 only up to 50 N) of the various polymorphs and the normalized values that strongly increase with the loads. As integrations are not allowed over unsteadiness such as e.g., kinks, these $W_{indents}$ (Table 1) were obtained by integration eqn. (4) from zero to first kink, then kinks to next kinks, and finally last kink to the chosen end. The variation of the indentation works is very large (>7 powers of 10, and normalized by a factor of 872). While the fcc (Fm3m) and bcc (Pm3m) polymorphs are well documented, only quantum chemical calculations predict higher pressure polymorphs with space groups Cmcm, Imma, and Pbcm [1]. Further possibilities for the sixth polymorph are perhaps the not predicted Pnma, twinning, or amorphous phase. There is yet no means for selecting and inserting another polymorph into the theoretical sequence of 3 polymorphs with increasing enthalpy.

The quantitative physical indentation allows for the determination of phase-transition energies, using the non-iterative elementary closed eqns. (5-7). The energy balance is calculated using W_{indent} kink by kink from Table 1 that is multiplied with 5/4 for obtaining the applied work $W_{applied}$ (5) and then the phase-transition work $W_{transition}$ (6) that is subtracted from the full applied work for all sections from zero to the kink value in the F_N-h loading curve [5]. Finally the whole transformation energy up to 50 N is obtained by summing up all sectional $W_{applied}$ contributions. The values and sums are listed in Table 2. For example the full $W_{applied}$ up to 50 N is the area of the triangle of zero to h_{max} of the F_N-h curve (119.235 μm), up to the final load (50N), and hypotenuse from zero to F_{max} (50N). Figure 1b when extrapolated to 50.00 N gives 2980.88 Nμm for full $W_{applied}$. The sum of all sectional $W_{applied}$ values is 2708.6913 Nμm (Table 2). The subtraction from full $W_{applied}$ (2980.88 Nμm) gives the full transformation energy from zero to 50.00 N as 272.189 Nμm. This is remarkably 9.13% of the indenter work: the indenter has to provide that work for the 5 endothermic phase-transitions to occur up to 50.00 N load.

NaCl transi-tion onsets	h_{kink} (μm)	$W_{applied}$ (Nμm)	$\Sigma W_{applied}$ (Nμm)	Full $W_{applied}$ (Nμm)	$W_{transition}$ (6) (Nμm)	Normalized $W_{transition}$ (Nμm per μm)
fcc to kink[a]	0.1909	$4.8639 \cdot 10^{-5}$	$4.8639 \cdot 10^{-5}$	$5.8988 \cdot 10^{-5}$	$1.0349 \cdot 10^{-5}$	$5.4212 \cdot 10^{-5}$
fcc to bcc[a]	0.69784	$95.8437 \cdot 10^{-5}$	$1.007076 \cdot 10^{-3}$	$1.4790 \cdot 10^{-3}$	$0.471924 \cdot 10^{-3}$	$0.6763 \cdot 10^{-3}$
bcc to #3	20.80762	26.95876	26.959767	27.018690	0.058923	$2.8318 \cdot 10^{-3}$
#3 to #4	45.01300	170.21126	197.17103	205.22778	8.05675	0.1790
#4 to #5	82.89834	755.86927	953.04030	1012.29245	59.25215	0.7148
#5 up to 50N (capped #6)	120.8539	1755.6510	2708.6913	2980.88	272.189	2.2522

[a]Indented with Berkovich [4].

Table 2: The arithmetically obtained applied and transition energies of the various NaCl polymorphs upon depth sensing nano to macro indentation with the Vickers indenter.

The energy treatment provides variations up to 3.61×10^7 ($W_{applied}$), 5.05×10^7 (full $W_{applied}$), and 2.63×10^7 fold ($W_{transition}$) of the different works (the capping of the #6 value at 50.00 N load is arbitrary, not related to a physical event). All of these 4 phase-changes of NaCl are endothermic. The contributions of the normalized transition works (Nμm per μm) are also strongly increasing with the load by a factor of 4.15×10^4 (Table 2). We deal here with the polymorphs that actually exist at the indenter interface for a characteristic load-range, in addition to the displaced phase-changes regions that, of course, continue to be shifted, more and more away from the tip interface with formation of their respective interfaces that may or may not be commensurate. Here we have no cracks around the tip but only very distant macro-cracks at very high load (Figures 3-6). This certainly complicates the meaning of the indentation moduli from the unloading curves, when the highly energetic polymorphs revert to the stable halite (fcc).

Inverted shape of the residual impressions

Impressions are better imaged in the inverted pyramidal form and as sharp projection of their 3D-images for better looks at their height and surfaces. This helps to qualify the surface appearances (Figure 3). The side faces are mostly smooth, but there is always some material on the impression faces, small at the lower load and larger at the higher and highest loads. The edges and apices are always rough and thus clear indications of reverting NaCl polymorphs. Particularly the 20 N (cubic to brick-like) and 50 N inverted impressions (less so also at 5 N) reveal crystallization at the apex (actually depth) and at the edges. This confirms the obvious corresponding polymorph reversions. The regular structures that cover the edges are also seen in the 2D-projections and these differ from each other, due to the varying number of reverting polymorphs. Upon 10 months storage, the features along the rims completed their crystallization giving linearly aligned cubes each with 7 μm side lengths; most of them almost perfect to both sides in the horizontal direction of Figure 3c. The depth of the 50 N impression stays at measured 110 μm; most of the side faces remain smooth. The white areas augmented 4 to 5 fold, but their maximal height of 6 μm towards the indentation surface was not superseded (these are, of course, depressions at the inverted Figure 3). This augmentation upon long storage excludes their being surface defects of the indenter. The darker areas remained less than 1 μm high giving more straylight than the white ones. Moisture influence is thus very unlikely, as that would have influenced the extremely small (< 1 μm) crack lines in Figure 6a, below.

On-site studies with highly focused X-ray diffraction would appear promising for verification of the theoretically predicted structures and for the elucidation of the sixth polymer's structure.

Cracking behavior

The lack of any radial or lateral cracks at the indenter tip interfaces

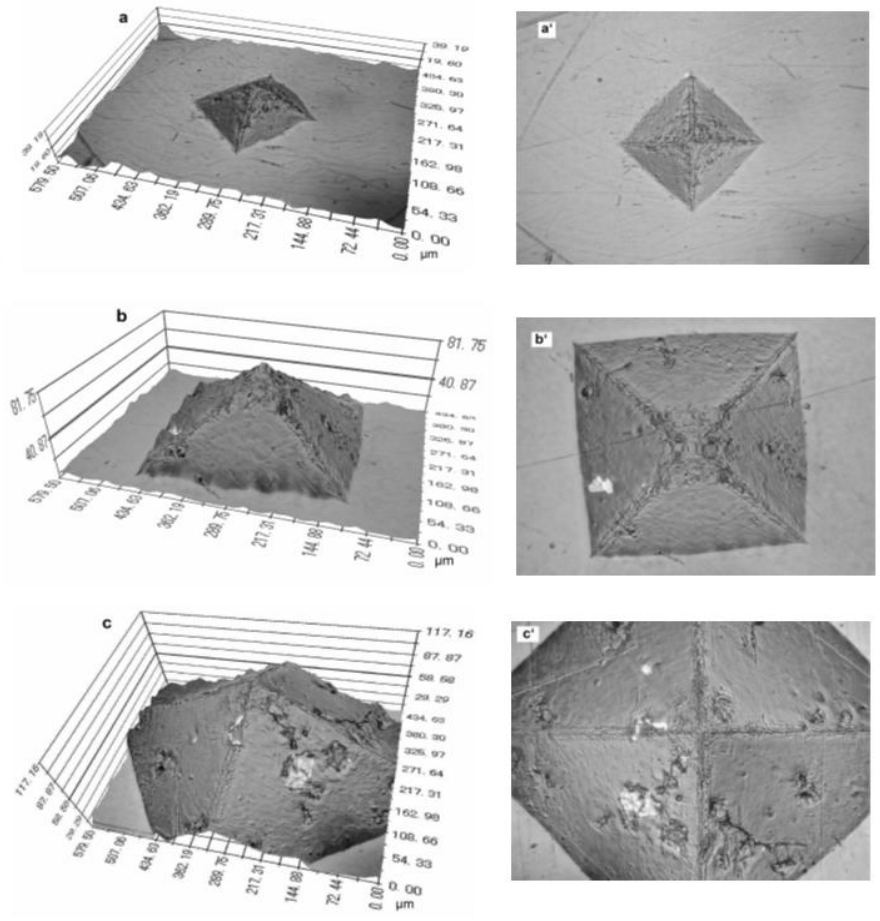

Figure 3: 3D-microscopic images of inverted residual impressions, and their projections (a,a') 5 N, h_{max} 31 μm; (b,b') 20 N, h_{max} 78 μm; (c,c') 50 N, h_{max} 115 μm.

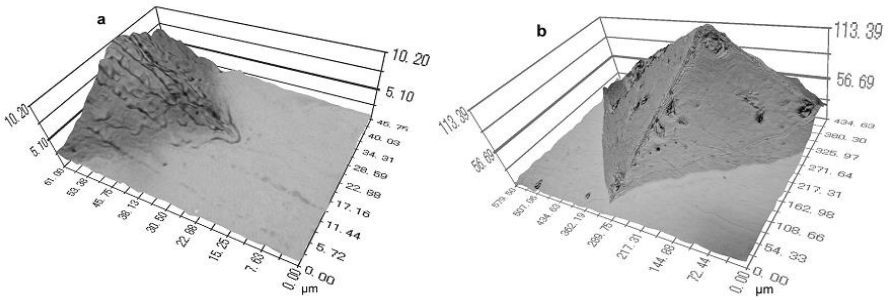

Figure 4: 3D-microscopic inverted corner images of indented NaCl with the apices capped of (a) residual 20 N impression (5000X lens; 14 x 1-μm focal distance images composed), (b) 50 N impression (500X lens; 28 x 5-μm focal distance images composed), showing the distinct end at the corners, excluding any radial cracking.

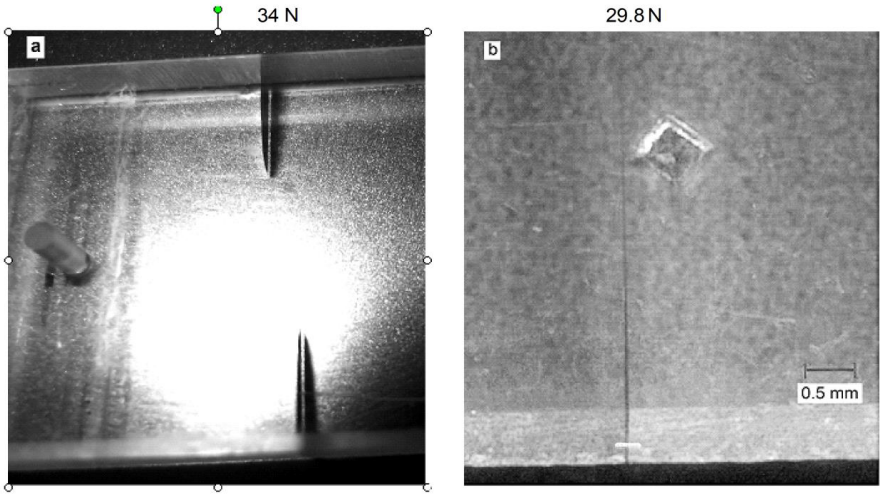

Figure 5: (a) Flash photo on (−100) of NaCl at 29,8 and 34 N at the 50 N indentation, showing both cracks enhanced by the shadows; (b) microscopic 2D-image with 25X lens on (−100), showing both the base of the impression on (100) shining through from underneath and the crack on (−100); unfortunately the actual stop of the crack after 2/3 of the front face could not be shown by the 2D-microscope with vertical illumination in reflection mode. The crack ends at the white bar that was added.

up to 50 N load and 120 μm depth is surprising in view of the multiple phase-changes. It is not only due to a high ductility, but also to an apparently reasonable compatibility between the adjacent polymorphs, as these are formed. This is already seen from the fact that the bcc NaCl volume undergoes a considerable decrease from 27.6 to 17.6 A^3 at 300 K, when the pressure in an anvil cell is increased from 30.6 to 180 GPa [22]. Furthermore, the experimental fcc → bcc volume drop of 5.7% [23], and the small predicted volume drops from first-principle calculated polymorphs of 5.03% (fcc → bcc), 1.19%, 0.92%, and 0.33% [1], are also judged helpful for avoiding cracks. Figure 4 proves the absence of radial cracks with highest precision by 500X and 5000X lens 3D-microscopy. This excludes calculation of common fracture toughness values. Also lateral cracks were not seen on careful visual inspection of the fully transparent sample. Importantly, the absence of cracks from the corners is still retained after 10 months storage (50 N impression with 5000X lens).

Only two large cracks formed at short sequence in the 30 N regions, far away from the indenter corner, but only at the opposite side of the 6.3 mm thick sample. They happened when the depressions of Figure 1b occurred. The exclusive formations of 5.8 and 6.9 mm long cracks on (−100) of sodium chloride along the (00−1) cleavage planes (with respect to (100) for the indentation) at the extreme loads of 29.8 and 34.0 N when reaching 92.94 and 97.31 μm indentation depth (Figure 1b) are unusually far away from the actual impression. Figure 5a shows a flash-light photo of the (−100) surface (opposite to the impression side). These cracks are enhanced by the so generated shadows. The top one ends at half of the outer sample depth, the bottom one at about 2/3 of the sample depth of 6.3 mm. The distance between the crack planes is 1.89 mm.

The 2D-microscopic image with a 25X lens (Figure 5b) shows the 50-N indent from the backside (coming up) with its basal diameter of 0.815 mm. For technical reasons the stop of the crack at 2/3 of the front face (a white bar has been included) cannot be shown by the 2D microscope with vertical illumination at reflection mode in Figure 5b. The distance of the indent to the sample edge is 3.32 mm. The distance from indent's center to the (00−1) planes of the cracks is 0.18 mm and 2.07 mm, the distances to the start of these cracks on their surfaces are 6.15 and 13.31 mm, respectively. The cracks reach a maximal width of 11.2 and 7 μm towards their exits, where their depths are 3.15 and 4.2 mm down with end-widths at the 1 μm range. The very far distances of the cracks from the indentation and none of them at the indenter deserve a closer inspection (Figure 6).

As already mentioned in the Hardness, Modulus, and Polymorphs Section, the long-range crack formations are responsible for the depressions in the Figure 1b. The miniscule depression at 28.5 N preceding the first more important one at 29.8 N provides an important clue for the nucleation event. Clearly, there must have been a primary cracking trial and that is seen in Figure 6a with the 6.15 mm distant nucleation that appeared first. It shows the interrupted nucleation (position 2) that grew from a very narrow tail along a (00−1) plane, apparently starting at an about 20° inclined interface of polymorphs, reaching 1.64 um width, but shortly thereafter ceasing, again along (00−1). Shortly thereafter it resumed, formed a grain that still seemed to have some problems for proceeding, but it was finally successful (position 1 in Figure 6a), without interruption till the exit. It rapidly reached 4 µm width, narrowed to 1 to 1.5 µm after 150 µm and again after 280 µm (both for about 30 µm length), and more or less continuously assumed 4 to finally 11.2 µm width till the exit. All of that strictly keeps with the (00−1) cleavage plane without any sidewise branching to the equally packed (0−10) cleavage plane (Figure 6c). And all details of the nucleation (including the slight imperfections of the surface at 5000X enlargement) were precisely reproduced after 10 months storage of the sample. This confirms the cracking from an interface exit of different polymorphs, as pushed away from the indenter by increasing load, where it coincided with a (00−1) cleavage plane. It proceeded along with it by using part of the flatly upcoming (about 20°) interphase.

Apparently, the first macroscopic cracking produced enough stress for triggering the common but still highly hindered nucleation at the 13.31 mm distance from the indent around a thus formed grain, as shown in Figure 6b. This second crack continues from there with 2 µm width for 1 mm length where it interrupts 12 times giving parts with 0.6-2 µm width all along (00−1). From there it resumes continuously first with 2-3, then 4-5, and 5-7 µm width till its exit at 6.9 mm length, again strictly along the (00−1) plane. This must not have been happening along an interface of polymorphs at so far distance from the indent. This more distant crack is thus taller than the closer one. The 12 interruptions after 1 mm length indicate again the difficulties for such cracking of the optical NaCl single crystal. Figure 6d again shows the smooth run without side branching.

Discussion

Indentation hardness and modulus

The depth-sensing indentation answers from the transparent NaCl model are particularly reliable, because there were no distortions by cracking emanations from the indenter up to 50 N loads. The first physically defined linear regression hardness H_{phys} should gain increased application value at the expense of unclear indentation moduli E and their false equalization with Young's modulus by the ISO standard 14577. Due to their different physical meaning any numerical resemblance between unidirectional Young's modulus and the ISO or physical indentation modulus is at best fortuitous [9]. The disregarded change by phase transitions and poor repeatability of unphysical E_{ISO} are particularly troublesome, as numerous mechanical properties are continuously deduced from E_{ISO} [9]. For example, they are used as finite element iteration input. Also, the still multi-directional indentation moduli $E_{r\text{-}phys}$ values in Table 1 (bcc NaCl: 32.245 mN/µm²) can not be compared with published experimental or first-principle calculations of for NaCl (fcc: 53.466, bcc: 75.615 GPa), or experimental bulk moduli (fcc: 23.40 to 26.40 GPa; bcc: 26.60 GPa) [21,24,25]. The steep pressure dependences of unidirectional Young's moduli or bulk moduli (from constant hydrostatic pressure) are not comparable with the pressure changes at a retracting indenter. For example, the first-principle calculations predict for the transition pressure (30 GPa) E_{Young} values of 300 GPa for fcc NaCl and 210 GPa for the bcc polymorph. The latter value is predicted to increase to 350 GPa at 70 GPa pressure. Also, the

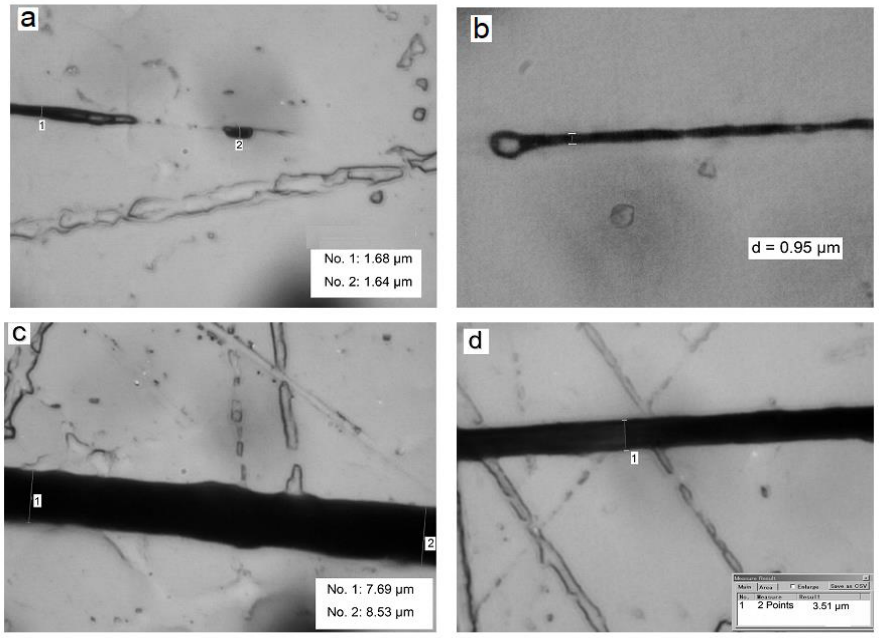

Figure 6: Optical 3D-microscopic projection images (5000X lens) of the cracks' nucleation details on sodium chloride; the widths of the rectangles are 76x 55 µm; (a) the less distant from indention crack at 28.5 and 29.8 N load with an interruption, (b) the more distant from the indention crack as nucleated from a grain at 34.0 N load; (c) first crack (5000X lens) at 3.2 mm of its length; (d) second crack (5000X lens) at 1.7 mm of its length, also showing its smoothness.

calculated bulk and shear moduli are predicted to steeply increase with applied pressure [21]. And there is also the temperature dependence with heated materials. To learn more about the elasticity behavior upon unloading, it might be useful to very carefully study the unloading rate dependences within every phase transition onset ranges. Reliable elastic moduli for materials at high pressures combined with high temperature are certainly required. The indentation modulus situation is very confusing indeed and one should always take into account, whether an elastic modulus types' use is for length- or volume-related properties. ISO and ASTM add most severely to this confusion with indentation moduli by not detecting or appreciating the phase-transition onsets (Table 1). This creates high risks for the widespread use of E_{ISO}, including thereof deduced and calculated other mechanical parameters (more than 10, from adhesion to toughness) [9]. *These unacknowledged daily-life risks derive from formation of interfaces between polymorphs, facilitating crack nucleation.* They must be discontinued and replaced by reliable physical techniques.

Indentation $E_{r\text{-}phys}$ moduli reliably characterize pristine materials only before the first phase transition onset, but they are also not Young's moduli. Unlike $E_{r\text{-}phys}$, the linear regression hardness H_{phys} (penetration resistance k, the slope of the so called Kaupp-plot) values from depth-sensing indentations (2) favorably govern the energetics (Tables 1 and 2), detect other important material's properties (e.g. surface effects, gradients, inter-layers, cracks, adhesion effects, phase transitions, exclusion of one-point invaluable measurements), and are most promising for further unprecedented applications.

Phase transition and unusual cracking

The sharp phase transition onset at the kink position – of with Kaupp-plot (1) analyzed loading curves – succeeds with on-site Raman spectroscopy, electron diffraction, X-ray, and electric conductance, or other physical techniques, both in hydrostatic and indentation experiments. Most studied are the phase-transitions of NaCl and silicon with various methods that fit nicely together. This is already reviewed in reference [4]. After the unloading all energetic polymorphs must have reformed the halite structure, at the edges as cubes, and at some face sites probably as sub-micro crystallites. One should however check, whether these features would be amorphous or twinned NaCl instead. This might perhaps open up another technique for achievement of twinned NaCl (cf for references of NaCl twinning) [4]. Pressure induced cracking is generally facilitated by phase transitions. The transparent and phase-transforming NaCl is nevertheless crack-resistant for depth-sensing macro indentation. This is favorable for the demonstration of the sequence of phase-transitions, yielding reliable results. It allows for characterizing the polymorphs energetically with respect to work of indentation within their loading range and thus for obtaining the transformation energies. These important data required correct physical data and appreciation of the physically correct closed eqns. (1-7). The arithmetic covers multiplications, integrations, summations, and subtractions. The detection of phase-transition energies by checking the energy that is lost for an endothermic case (to be provided by the indenter), or won for an exothermic case (to help the indenter), is a major advance in mechanical physics [5]. The obtained results show better than the also determined H_{phys} and $E_{r\text{-}phys}$ values how strongly these vary from kink to kink. It turns out that the pressure and plasticity including phase transformations is being distributed over very long distances in macro-indentations. Clearly, every more energetic polymorph zone at the indenter shifts all earlier energetic zones with their lower energetic polymorphs more and more away. This adds a new interface after every new phase transition onset. Any one of these may facilitate nucleation of long-range cracks. On the other hand, phase transition with volume drop helps to prevent cracks originating directly from the indenter, as in this case. The unusual cracking behavior of NaCl deviates from the common radial, lateral, median, and combined types of strongly incommensurable polymorphs of brittle materials. The main reason for the non-cracking at the Vickers indenter within NaCl, up to 50 N loads appears to be the marked volume decrease under pressure. Volume decrease of 35% was reported for the first fcc → bcc transition at the hydrostatic transformation pressure of 29.1 GPa [26]. Figure 6a clearly indicates that phase transitions under load and temperature stress have to be avoided in materials of technical use. Uncountable transformations and reversions in strained objects above and below the transformation force create a risk for crack nucleation by always forming polymorph interfaces. Thus, the transition onset must be determined via Kaupp-plot and defined as maximal allowance of the material in revised ISO/ASTM Standards.

One-point industrial indentations

The most important flaw of ISO and ASTM standards is their non-consideration of phase-changes that are of outstanding importance for the reliable characterization of the original material (before the load at phase-transition onset). The occurrence of sequential multi phase-changes with always higher energetic polymorphs is particularly troublesome for industrial one-point macro-indentions (HV, HK, HB, HR, shore, LH, and more specialized hardness values) at very high loads [10]. The first phase-changes occur already in the μN and mN ranges, and unrevealed multiple phase-changes inevitably occur at the very high loads that falsify the mechanical descriptions and facilitate materials' failures. These problems must be urgently avoided for industrial products that are used under high pressure stress. The present work underlines it with the study of highly crack-resistant sodium chloride as a suitable very simple cubic model system, exhibiting four consecutive phase-changes (only two of them were already known) and an unusual type of cracking. 50 N (corresponding to HV5) is still low for the "common" Vickers hardness load range of 40-980 N (HV 4-98) and may extend up to 1500 N (HV 150). But also the lowest loading region of 0.1 N to 40 N (HV 0.01-HV 4) cannot avoid phase changes [10]. Only the depth-sensing macro-indentation and nano-indentations can reveal the phase-transition onsets (1). Theoretical calculations do not help, if they predict mechanical parameters that are far off the experimental results.

Long-range cracking nucleation

The complete absence of radial, median, half-disc, and horizontal cracks at the Vickers indenter up to 50 N force upon NaCl at the expense of 5.8 and 6.9 mm long cracks along the (00−1) planes at large distance is unusual (Figure 5). The cracks at the very high loads of 29.8 and 34.0 N loads represent a new cracking type that is highly resolved by the 3D microscopy. The depressions in Figure 1b indicate the time of cracking, and that the first one had a two-step nucleation, due to the miniscule pre-depression. Both cracks start on the opposite surface, 6.15 and 13.31 mm away from the residual 50 N indentation, onto the 6.3 mm thick single crystal. The difficult nucleation of the less distant first crack, obviously at an interface between two different polymorphs under load, in Figure 6a starts with a very narrow (<< 1 μm) scratch along (00−1) providing 1.64 μm width, but shortly thereafter it is reverting to such tiny scratch and resuming with a new trial that is finally successful strictly along (00−1). No branching into (0−10) or (−100) (Figure 6a) occurs. The interfaces of the polymorphs occur

about 20° inclined, and this concurs with the self-evident formation of phase transition interfaces. This happens away from the indenter further and further, as the load increases, and more so from the edge sides and apex of the indenter.

The more distant second crack has been announced by the final depression of the loading curve (Figure 1b). It was evidently triggered by the first macro-crack and has a common non-interrupted nucleation from around a grain, as seen in Figure 6b. It runs smoothly with 2 μm width but experiences trouble after 1 mm length with 12 interruptions within 90 μm of the length, but still strictly keeping with the once selected cleavage plane, and finally resuming uninterrupted with widths from 4-7 μm for a total of 6.9 mm. The value of highly resolving 3D-microscopy for such detailed knowledge is evident. The right/left bias in the present experiment is by chance (both are on the left side in Figure 5). This may not be surprising for the second crack as triggered by the first one, but there are four corners of the tip and all orthogonal directions have identical cleavage planes in the cubic crystal lattice. The reasons may be some unavoidable miniscule deviation of perfectly normal indentation and the unavoidable wedge apex orientation of the four-sided Vickers pyramid. Disorder of this single crystal structure with extraordinary high crack-resistance appears a less probable choice than finding a coincidence of polymorphs' interface exit with cleavage plane. In so far, the orientation bias of the cracks will probably differ in future experiments.

Prospects for polymorphs' structure determination

The inverted 3D-images of the impressions and their 2D-projections retaining the depth sharpness yield important new information. Their surfaces are not completely flat but confirm the phase-changes into unstable polymorphs at the apices (deepest impression points) and particularly at the edges of the indentation with the reversions upon the unloading. These appear to partly crystallize into cubic halite features, which is best seen in Figures 3b and 3b' as brick-like or cubic objects. The by necessity fast reversions explain the different appearance of the ordered structures from the different polymorphs that only exist under load. The apparent crystallite formations are thus promising for onsite X-ray crystal structure determinations under load with sharply focused X-ray diffraction studies, which is an important task for the future.

The high energy transformations starting at 2.487, 9.1186, and 24.4284 N (in addition to the 2 two known ones, giving a total of six polymorphs) are now found experimentally. But recent first-principle calculations predicted only three higher energy polymorphs with Cmcm, Imma, and Pbcm structures (describing only five polymorphs). The respective volume drops starting with the basic halite structure are predicted to 5.03%, 1.19%, 0.92%, and 0.33% [1]. We cannot locate the sixth experimentally found unstable polymorph that could be Pnma, twin, or amorphous. The missing color changes up to 50 N loads leave questions, whether ionic with metallic character of NaCl is in fact present in the pressurized predicted Cmcm, Imma, and Pbcm polymorphs [1]. Measurements of electric conductance upon similar depth sensing macro-indentation are our next task for clarifying these points.

Conclusions and Applications

Indentation is not only hardness and indentation modulus. The iteration-less physical treatment of indentations opens several new advents and improves the techniques' importance. The present work uses NaCl as favorable ductile standard material to reveal a sequence of polymorphs by depth-sensing macro-indentation at forces that would be used for Vickers hardness values of HV 0.5, 2, and 5. The NaCl single crystal profits from full transparency and surprising crack-resistance. New mechanical parameters are revealed, such as physical hardness H_{phys}, physical indentation modulus (avoiding iterations!) $E_{r\text{-}phys}$, phase change onset data, indentation work W_{indent}, and phase transition work $W_{transition}$ for all transformation steps with normalized transition work, and unexpected remote crack-nucleation details. This includes measurements of activation energies of phase transitions from temperature dependent indentation loading curves for the NaCl fcc → bcc transition, as already published in 2014 [4]. All of that is only possible by using the physically founded universally valid closed eqns. (1-7), rather than iterations.

Six different NaCl polymorphs have been identified by their onset load and transition energies. In addition to fcc and bcc, first principle calculations predicted structures for three of them, proposing both ionic and metallic behavior [1], but we could not see color or metallic reflection up to 50 N load (final clarification of theoretically predicted NaCl metallization requires on-site electric conductance measurements that is planned). There remains the sixth polymorph to be energetically arranged. The surface shapes of the inverted residual impression images from 3D-microscopy furnish highly resolved images. These depict the reversion into halite (fcc) with clear signs of crystallization during the unloading at the (inverted) apex and tip edges. This makes on-site structure determinations with highly focused X-ray diffraction promising. The enormous crack-resistance of the single crystal NaCl withstands 50 N loads around the Vickers indenter without any trace of cracking at 5000-fold magnification with 3D microscopy of the inverted residual impressions. Only very distant long-range cracks have been localized in the 30 N regions and analyzed with highly resolving 3D-microscopy.These did not obstruct the further data regression up to 50 N. The strongly varying H_{phys}, $E_{r\text{-}phys,}$ W_{indent}, and $W_{transition}$ values in the force ranges of the Tables 1 and 2 provide an idea about the huge errors of the not depth-sensing single-force macro-indentation techniques, according to ASTM Standards that do not acknowledge that pristine materials exist only up to the first phase-transition onset load. Severe errors are also occurring when phase transfer onsets are not determined or disregarded by the ISO Standard 14577 for nano- and micro-indentations. These prescribe the still common double multi-parameter iterations on the basis of wrong exponent on the indentation depth, disregard (1), and still violate the principal energy law. The determination of the correct exponent 3/2 on h (1) from the loading data is a matter of <1 minute when loading them to Excel and calculating the Kaupp-plot (eqn. (1) is finding any F_a correction term) [3]. When however innocent graphical integration of a loading curve deviates from the mathematical 5/4 requirement of eqn. (5), this must not be used for questioning (5). On the contrary, such undue habit would be a new technique for the initial search of phase-transitions occurring under load, by avoiding data point's collection from published old loading curves for the Kaupp-plot. This can be demonstrated with an undue trial calculation: when the loading curve of Figure 1b (not regarding the depressions) would be graphically integrated despite the 4 phase-change unsteadiness kinks (part of them are shown in Figure 2), and if such "result" would be compared with the applied work according to (5), the ratio "$W_{applied}$"/"W_{indent}" would come out as "1.3857" but not 1.250 and therefore confirm the actual phase-changes. Clearly, the physically sound eqn. (5) must not be questioned by faulty integration over phase-change kinks' unsteadiness, but we can so rapidly obtain initial phase change information from innocently published previous loading curves for further studies.

This work shows that only the now first physically defined nanoscale hardness H_{phys} is precisely obtained by linear regression at loads before phase-change offsets. Only that characterizes the pristine material up to permissible load stress for its risk-reduced application, often within nano-indentation, exceptionally at first within micro-indentation. The H_{phys} importance will therefore increase at the expense of unphysical H_{ISO} and troublesome E_{ISO} indentation modulus. Also ASTM standard one-point HV, HK, HB, HR, Shore, LH, etc hardness values are unphysical as they do not consider the correct exponent 3/2 on h, violate the energy law, and disregard the multiple phase changes (also occurring at the calibration plates). These fast techniques must rather be complemented by depth-sensing macro-indentations with hitherto scolded Kaupp-plot (eqn. (1)) analysis, and supplemented with nano-indentation. This detects the most important phase-change onsets. Polymorph interfaces facilitate the nucleation of cracks with severe failure risks. When the phase changes are irreversible (e.g., α-SiO_2 to amorphousness [5]) the material might immediately fail. In the reversible case, cracks might occur after numerous transformations back and forth. This will ask for different materials or for addition of particular mediation agents that increase the load for phase-change onsets. But this must be controlled with depth sensing physical indentation analysis. Also the alternation of minor reversible endothermic and exothermic phase changes might be helpful. For example, this could be shown up to 700°C with the famous ODS super-alloy INCOLOY$^{(R)}$ MA 956 (but only up to 5 mN) that exhibits alternating almost equally important endo- and exothermal phase change onsets in the Kaupp-plot [27,28]. Conversely, the $Fe_{43}Cr_{16}Mo_{16}C_{15}B_{10}$ super-alloy gave a strong endothermic transition at 72.4 mN und 0.495 µm at RT (two linear branches, Berkovich, up to 260 mN). Radial and horizontal cracks emanating from the impacting tip (these might also start upon the pressure release) must also be suppressed. Most high pressure polymorphs are unstable and additional thermal stress must also be considered with activation energy measurements of the phase-changes [4]. It is therefore highly relevant having exemplified the situation with a material exhibiting four phase-changes with a total of six energetically characterized polymorphs, not distorted by cracking up to 50 N load. Only a new type of cracking (far away from the indenter on the opposite sample side) occurred in the 30 N load region (corresponding to HV 3). Such type of cracking might escape visual recognition in opaque materials. It is only indicated in the depth-sensing loading curve by small depressions as in Figure 1b. These are also indispensable diagnostic tools. Thus, industrial depth-sensing macro-indentations, as supplemented by nanoindentation, appear as urgent tools for the failure fighting management to avoid unnecessary risks of technical products; urgently requiring revised ISO/ASTM Standards. Failures of materials have undoubtedly physical reasons. Mechanical parameters must therefore correspond with physics!

Acknowledgements

We thank Dr. Ehrhard Reimann from Zwick GmbH & Co KG Ulm, Germany for providing access to the depth sensing Zwick/Roell ZHV Zwicky Z2.5 macro region instrument and Stephanie Rösner for her experienced running the instrument at the NaCl macro-indentations according to the author's on-site wishes.

References

1. Chen X, Ma Y (2012) High-pressure structures and metallization of sodium chloride. EUROPHYS LETT 100: 26005-26008.
2. Thurn J, Morris DJ, Cook RF (2002) Depth-sensing indentation at macroscopic dimensions. J Mater Res 17: 2679-2690.
3. Kaupp G (2016) The physical foundation of $F_N = k\ h^{3/2}$ for conical/pyramidal indentation loading curves. Scanning 38: 177-179.
4. Kaupp G (2014) Activation energy of the low-load NaCl transition from nano indentation loading curves. Scanning 36: 582-589.
5. Kaupp G (2013) Penetration Resistance: A new approach to the energetics of indentations. Scanning 35: 392-401.
6. Korth Kristalle Ltd. (2018) Itenholz-Kiel, Germany.
7. Fei Y, Ricolleau A, Mibe K, Shen G, Prakapenka V (2007) Toward an internally consistent pressure scale. Proc Natl Acad Sci 104: 9182-9186.
8. Kaupp G (2017) The ISO Standard 14577 for mechanics violates the first energy law and denies physical dimensions. J Mater Sci Engin 6: 321-328.
9. Kaupp G (2017) Dilemma between Physics and ISO elastic indentation modulus. J Mater Sci Engin 6: 402-405.
10. Kaupp G (2017) Challenge of industrial high-load one-point hardness and of depth sensing modulus. J Mater Sci Engin 6: 348-354.
11. Kaupp G, Naimi-Jamal MR (2013) Penetration resistance and penetrability in pyramidal nano indentations. Scanning 35: 88-111.
12. Kaupp G, Naimi-Jamal MR (2010) The exponent 3/2 at pyramidal nanoindentations. Scanning 32: 265-281.
13. Boussinesq J (1885) Applications des potentiels a l'etude de l'equilibre et du mouvement des solides elastiques. Gauthier-Villars, Paris, France.
14. Love AEH (1939) Boussinesq's problem for a rigid cone. Q J Math (Oxford) 10: 161-175.
15. Sneddon IN (1965) The relation between load and penetration in the axisymmetric Boussinesq problem for a punch of arbitrary profile. Int J Engn Sci 3: 47-57.
16. Oliver WC, Pharr GM (1992) An improved technique for determining hardness and elastic modulus using load and displacement sensing indentation experiments. J Mater Res 7: 1584-1583.
17. ISO (International Organization for Standardization). ISO 14577. Available from the member of the particular country; for USA: American National Standards Institute, 25 West 43rd Street, Fourth Floor, US-New York, NY 10036-7417.
18. Naimi-Jamal MR, Kaupp G (2005) Quantitative evaluation of nanoindents: Do we need more reliable mechanical parameters for the characterization of materials? Int J Mater Res (Z. Metallkd) 96: 1225-1236.
19. Troyon M, Abbes F, Garcia Guzman JA (2012) Is the exponent 3/2 justified in analysis of loading curve of pyramidal nanoindentations? Scanning 34: 410-417.
20. Merle B, Maier V, Durst K (2014) Experimental and theoretical confirmation of the scaling exponent 2 in pyramidal load displacement data for depth sensing indentation. Scanning 36: 526-529.
21. Lu C, Kuang XY, Zhu QS (2008) Characterization of the high-pressure structural transition and thermodynamic properties in sodium chloride: a computational investigation on the basis of the density functional theory. J Phys Chem B 112: 1389-1395.
22. Ono S (2010) The equation of state of B2-type NaCl. J Phys Conf Ser 215: 012196-012208.
23. Bassett WA, Takahashi T, Mao HK, Weaver JS (1968) Pressure-induced phase transformation in NaCl. J Appl Phys 39: 319-325.
24. Birch F (1985) Finite strain isotherm and velocities for single-crystal and polycrystalline sodium chloride at high pressures and 300°K. J Geophys Res 83: 1257-1268.
25. Bukowinski MST, Aidun J (1985) First principles versus spherical ion models of the B1 and B2 phases of sodium chloride. J Geophys Res 90(B2): 1794-1800.
26. Piermarini GJ, Block S (1975) Ultrahigh pressure diamond-anvil cell and several semiconductor phase transition pressures in relation to the fixed point pressure scale. Rev Sci Instrum 46: 973-979.
27. Kaupp G (2018) Basic physics disproves the obligatory ISO-14577 standards: a dilemma for all indentation mechanics.
28. Kaupp G (2017) ISO violates the first energy law including hardness/elasticity standards from indentations: What can be done?